

Simultaneous spectra and radio properties of BL Lac's

M. Mingaliev^{1,2}, Yu. Sotnikova^{1*}, T. Mufakharov³, E. Nieppola^{4,5}, M. Tornikoski⁴, J. Tammi^{4,6}, A. Lähteenmäki^{4,6}, R. Udovitskiy¹, and A. Erkenov¹

¹ Special Astrophysical Observatory of RAS, Nizhnij Arkhyz, 369167 Russia
e-mail: marat@sao.ru

² Kazan Federal University, 18 Kremlyovskaya St., Kazan, 420008, Russia

³ Shanghai Astronomical Observatory, Chinese Academy of Sciences, Shanghai 200030, China

⁴ Aalto University Metsähovi Radio Observatory, Metsähovintie 114, 02540 Kylmäla, Finland

⁵ Finnish Centre of Astronomy with ESO (FINCA), University of Turku, Väisäläntie 20, FI-21500 Piikkiö, Finland

⁶ Aalto University Department of Radio Science and Engineering, P.O. Box 13000, FI-00076 Aalto, Finland

Received XXXX, accepted XXXX

Published online in Astronomische Nachrichten, DOI 10.1002/asna.201713361

Key words galaxies: BL Lacertae objects: general – galaxies: active – radio continuum: galaxies

We present the results of nine years of the blazar observing programme at the RATAN-600 radio telescope (2005-2014). The data were obtained at six frequency bands (1.1, 2.3, 4.8, 7.7, 11.2, 21.7 GHz) for 290 blazars, mostly BL Lacs. In addition, we used data at 37 GHz obtained quasi-simultaneously with the Metsähovi radio observatory for some sources. The sample includes blazars of three types: high-synchrotron peaked (HSP), low-synchrotron peaked (LSP), and intermediate-synchrotron peaked (ISP). We present several epochs of flux density measurements, simultaneous radio spectra, spectral indices and properties of their variability. The analysis of the radio properties of different classes of blazars showed that LSP and HSP BL Lac blazars are quite different objects on average. LSPs have higher flux densities, flatter spectra and their variability increases as higher frequencies are considered. On the other hand, HSPs are very faint in radio domain, tend to have steep low frequency spectra, and they are less variable than LSPs at all frequencies. Another result is spectral flattening above 7.7 GHz detected in HSPs, while an average LSP spectrum typically remains flat at both the low and high frequency ranges we considered.

Copyright line will be provided by the publisher

1 Introduction

Active galactic nuclei (AGN) are unique objects in the Universe, because they are compact and extremely luminous. Their main observational properties can be explained by the presence of the super massive black hole at the centre of the galaxies, surrounded by an accretion disk and by fast-moving clouds. They come in different flavors all of which can be explained in terms of the so-called “unified scheme” (Urry & Padovani 1995), where the major difference between each of them is their orientation relative to the line of sight of the observer.

Blazars are the radio-loud subclass of AGN, characterized by strong non-thermal radiation across the entire electromagnetic spectrum (Kollgaard 1994; Perlman et al. 1998; Strittmatter et al. 1972). Strong variability at different timescales and wavebands is believed to be a result of relativistic motion of non-thermal plasma along the jet, oriented at small angles to the observers line of sight (Blandford & Rees 1978; Urry & Padovani 1995). The average value of viewing angle of blazars is about 5° according to the estimations made by Lister et al. 2013. The spectral energy distribution (SED) of blazars features two

broad components: the low-energy part (with the peak in the radio/infrared band) is believed to be formed by synchrotron emission and high-energy hump (with the peak in the gamma-rays) is usually explained in terms of inverse Compton radiation (e.g., Sambruna et al. 1996; Sikora et al. 1994) or hadronic processes (e.g., Mücke & Protheroe 2001; Petropoulou et al. 2015).

Blazars are commonly distinguished as low-synchrotron peaked (LSP), intermediate-synchrotron peaked (ISP), and high-synchrotron peaked (HSP), depending on the peak frequency of the synchrotron component (ν_{peak}^S) of their SED. In this paper we adopt a blazar classification from the Fermi-LAT 3LAC catalogue (Ackermann et al. 2015), which uses the common convention by Abdo et al. 2010 to classify a blazar as an LSP for $\nu_{peak}^S < 10^{14}$ Hz, ISP for 10^{14} Hz $< \nu_{peak}^S < 10^{15}$ Hz, and HSP for $\nu_{peak}^S > 10^{15}$ Hz.

Blazars are historically divided in two main classes according to the presence or absence of the lines in their optical spectra: BL Lacertae type objects (BL Lacs) have no lines or very weak ones (with the rest frame equivalent width $EW < 5 \text{ \AA}$), while flat-spectrum radio quasars (FSRQs) exhibit normal quasar-like spectra with strong broad emission lines (Stickel et al. 1991; Urry & Padovani 1995).

* sjv@sao.ru

Currently one of the most extensive list of blazars is presented in the Roma-BZCAT catalogue by Massaro et al. (2009). This catalogue is based on multi-frequency surveys and detailed checkout of the literature. The total number of blazars currently listed in the Roma-BZCAT (Edition 5.0) is more than 3500. But only a relatively small number of objects have been intensively observed at many frequencies simultaneously. The spectral coverage of many of them is poor, both in time and in frequency. Few observatories have long term monitoring programmes for blazars at radio wavelengths, Metsähovi Radio Observatory (Teräsraanta et al. 2004), University of Michigan Radio Observatory (UMRAO) (Aller et al. 1999), Owens Valley Radio Observatory (OVRO) (Richards et al. 2011) and INAF-Istituto di Radioastronomia in Medicina and Noto (Bach et al. 2007) are among them.

The RATAN-600 radio telescope has been monitoring AGN on regular basis for more than 10 years. In this paper we present observational results for 290 blazars obtained at six frequencies from 1.1 to 21.7 GHz with this telescope. The main objective of our research is to obtain multi-frequency information about radio properties of the blazar subgroups by using a single instrument and simultaneous measurements to exclude possible systematic errors as well as variability. This unique data that we collected allowed us to study the spectral properties for relatively large sample of blazars.

2 Sample

The sample consists of blazars - BL Lacs, BL Lac candidates, and blazars of an uncertain type - with flux density more than 400 mJy (added to the sample in 2012) and more than 100 mJy (added in 2014) at 1.4 GHz, selected from the Roma-BZCAT catalogue¹ (Massaro et al. 2009) maintained by the ASI Science Data Center. The first observations with the RATAN-600 started in early 2005 while the last sources were added to the programme in early 2014. The sample is heterogeneous and contains sources both faint and extremely bright in the radio domain. The median value of the flux density at 1.4 GHz is 0.3 Jy; the minimum value is 0.002 Jy at this frequency (MS 0122.1+0903); the maximum is 22.83 Jy (3C84). The inclusion of some FSRQs in this sample can be explained by ambiguity of blazar classification, as pointed out by Marcha et al. (1996) and Antón & Browne (2005), and some BL Lacs have been classified as FSRQ or vice versa (Shaw et al. 2012). Originally (in 2005) we observed some FSRQs as the BL Lac sources or BL Lac candidates. But in the blazars classification in the BZCATs later edition they were classified as FSRQs and we have included them as such in order to stick to an uniform classification. Since there are both blazars of uncertain type (27) and BL Lac candidates (12) in the sample, it will not affect the analysis of the three subclasses of blazars HSP, ISP

and LSP. Thus, the sample mainly consists of BL Lacs, BL Lac candidates, blazars of unknown type, and additionally 14 FSRQs.

All objects of the sample were classified as low-synchrotron peak (LSP), intermediate-synchrotron peak (ISP), and high-synchrotron peak (HSP) blazars: 197 of them were detected by Fermi-LAT and classified according to the 3LAC. For another 93 objects we have used the ASDC SED builder² to fit the synchrotron part of the SED with the second or third degree polynom and get its maximum. The logarithm of the synchrotron peak frequency was calculated in the rest frame. We did not classify two sources in our sample (PGC 59947 and BZB J1733+4519) because they do not have enough observational data points in their SED to extract the reliable $\log \nu_{peak}^S$ value. The source list includes 149 LSPs, 62 ISPs, 77 HSPs and 2 blazars with unknown SED type. The list of sources and their characteristics are presented in Table 6:

- Col. 1 – Source name,
- Col. 2–3 – R.A. and Dec (J2000.0),
- Col. 4 – Number of observing epochs at RATAN,
- Col. 5 – Redshift z ,
- Col. 6 – Logarithm of the synchrotron peak frequency ν_{peak}^S in Hz,
- Col. 7 – SED class from 3LAC, an asterisk was used to denote blazars, for which the values of $\log \nu_{peak}^S$ were calculated using ASDC SED builder,
- Col. 8 – AGN class from BZCAT (Edition 5.0) Massaro et al. (2015).

The redshifts for objects were mostly obtained from the Roma-BZCAT, and for some sources from Simbad³. Redshifts are known for 238 sources, which is a relatively large number, considering the difficulty of obtaining this information for BL Lacs. The redshift distribution is presented in Fig. 1. The redshift values range from $z=0.018$ to 2.277, with the mean equal to 0.45 and median to 0.36. Redshifts have not been measured for 52 objects; 13 of them are HSP objects, 8 are ISPs and 31 are LSPs.

3 Observations

The observations were carried out with the RATAN-600 radio telescope during 2005–2014. Systematic monitoring was carried out during the period 2006–2008 for roughly one third of the sources. Observations were done in the transit (meridian) mode with the north and south sectors of the antenna (Korolkov & Pariiskii 1979; Parijskij 1993). An angular resolution in this mode of observations depends on a declination a source being observed. The FWHM in right ascension (RA) is given in Table 1; an angular resolution in declination is three to five times worse than in RA. Sources were observed from 3 to 15 times in each epoch to increase

¹ <http://www.asdc.asi.it/bzcat/>

² <http://tools.asdc.asi.it/SED/>

³ <http://simbad.u-strasbg.fr/simbad/>

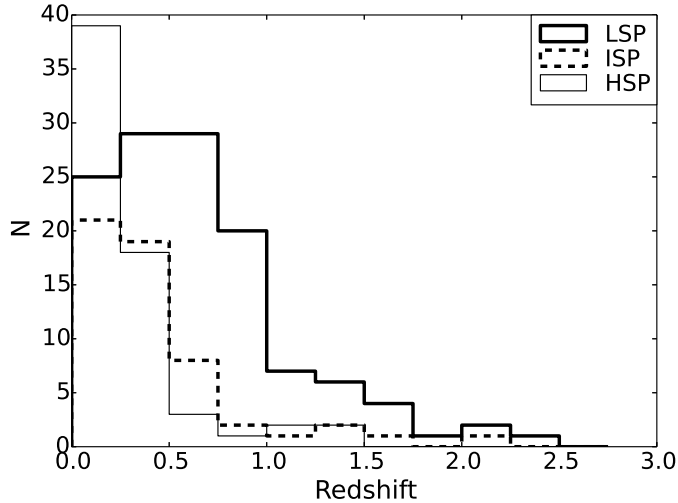


Fig. 1 Redshift distribution for different blazar subclasses of the sample.

the reliability of results and because of the weather or the receiver conditions.

Observations were carried out at six frequencies: 4.8, 7.7, 11.2, and 21.7 GHz (cryogenically cooled radiometers), and 1.1 and 2.3 GHz (uncooled radiometers). The 4.8 GHz cooled radiometer is a noise added radiometer (NAR), while other radiometers are designed according to the beam-switching scheme. All the radiometers were designed as the “direct amplification Dicke type” receivers. We use the data acquisition and controlling system for all continuum radiometers, as described by Tsybulev (2011).

The experimental data were processed with using the modules of the FADPS (Flexible Astronomical Data Processing System) standard reduction package by Verkhodanov (1997); this is a reduction system for data from the broadband continuum radiometers of the RATAN-600 secondary mirror. The processing methods are described in Mingaliev et al. (2007, 2012). The following eight flux density calibrators were used to calculate the calibration coefficients in the scale by Baars et al. (1977): 3C48, 3C138, 3C147, 3C161, 3C286, 3C295, 3C309.1, and NGC 7027. In addition, we used the traditional RATAN-600 flux density calibrators at low elevations: J0240–23, J1154–35, J0521+16, and the source J0410+76 at high elevations. Measurements of calibrators were corrected for angular size and linear polarization (where necessary), following the data from Ott et al. (1994) and Tabara & Inoue (1980).

The detection limit for RATAN-600 single sector is approximately 8 mJy under good conditions at 4.8 GHz and at an average antenna elevation ($\delta \sim 40^\circ$). At other frequencies the detection limit is presented in the Table 1. This value depends on the atmospheric extinction and the effective area on the antenna elevation H (from 10° up to 90° above the horizon) at the corresponding frequencies.

Table 1 RATAN-600 continuum radiometers. Where f_0 – central frequency, Δf_0 – bandwidth, ΔF – flux density detection limit per beam, and BW – beam width – an angular resolution in RA (an angular resolution in declination is three to five times worse than in RA).

f_0	Δf_0	ΔF	BW
GHz	GHz	mJy/beam	arcsec
21.7	2.5	70	11
11.2	1.4	20	16
7.7	1.0	25	22
4.8	0.9	8	36
2.3	0.4	30	80
1.1	0.12	160	170

The 37 GHz observations were made with the 13.7 m diameter Aalto University Metsähovi radio telescope, which is a radome enclosed Cassegrain type antenna situated in Finland (60 d 13' 04" N, 24 d 23' 35" E). The measurements were made with a 1 GHz-band dual beam receiver centered at 36.8 GHz. The HEMPT (high electron mobility pseudomorphic transistor) front end operates at room temperature. The observations are Dicke switched ON–ON observations, alternating the source and the sky in each feed horn. A typical integration time to obtain one flux density data point is between 1200 and 1600 s. The detection limit of our telescope at 37 GHz of the order of 0.2 Jy under optimal conditions. Data points with a signal-to-noise ratio < 4 are handled as non-detections. The flux density scale is set by observations of the HII region DR 21. Sources NGC 7027, 3C 274 and 3C 84 are used as secondary calibrators. A detailed description of the data reduction and analysis is given in Teraesranta et al. (1998). The error estimate in the flux density includes the contribution from the measurement rms and the uncertainty of the absolute calibration.

4 Results

4.1 Flux densities

The flux densities and the instantaneous spectra at several epochs of the sample sources (except the 37 GHz) are published in the BL Lac database⁴ maintained by the Special Astrophysical Observatory. The database is constantly updated with more data which is freely available and is described by Mingaliev et al. (2014).

Almost all sources have complete data at frequencies 4.8 and 7.7 GHz. When available, we also added near-simultaneous 37 GHz data from the Aalto University Metsähovi Radio Observatory database. The data were considered near-simultaneous if they were taken within two weeks of the RATAN observation. The occasional absence of data at certain frequencies is a result of data exclusion because of the partial resolution of a source at some frequencies, a source too weak to be measured reliably, a strong

⁴ www.sao.ru/blcat/

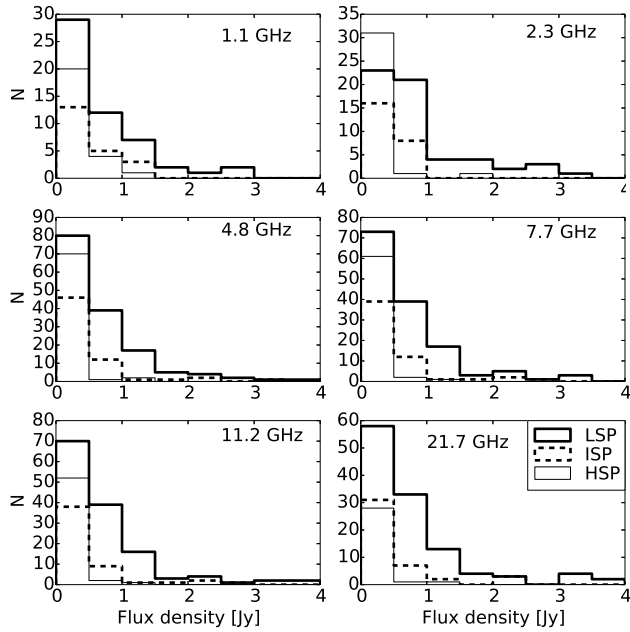


Fig. 2 The average flux density distribution at the RATAN frequencies by SED subclass (some bright sources with the average flux density above 4 Jy are excluded from the plot for the clarity of display).

influence of man-made interferences at 1.1 and 2.3 GHz, or due to strong interference from geostationary satellites at 11.2 GHz (between -10° and 0° degrees of declination). The values of the standard error of fluxes for the most sources are: 5-20 % for 11.2, 7.7, and 4.8 GHz, 10-35 % for 2.3, 1.0, and 21.7 GHz.

The distributions of the average flux densities by source class at all RATAN frequencies are shown in Fig. 2. We used a bin size of 0.5 with the middle value of the bin shown in the graph. The average flux densities have been calculated for $S/N > 4$ detections only. The sample sources are typically extremely faint, especially HSPs. Only one HSP (Mrk 501) in the sample has an average flux density reaching 1 Jy at most frequencies. This fact underlines the exceptional nature of this sample. Sources this faint are rarely targeted in observational campaigns, and never before have had their radio spectra determined this extensively.

The brightest source in the sample by far is 3C 84 ($S_{aver}=23.18$ Jy at 7.7 GHz, clearly more than the second brightest source BL Lac with 6.66 Jy). At 1.1 GHz 1828+487 is the brightest, but likely only because 3C 84 does not have data at that frequency (1.1 GHz observations were interrupted in 2012). The flux density of 1828+487 quickly decreases for frequencies higher than 1.1 GHz due to its steep spectrum. The medians of the average fluxes by frequency and class are listed in Table 2. The average flux density values are not drawn from the same distribution for the different SED classes according to the Kruskal-Wallis test. Pairwise comparisons confirm that LSPs are sig-

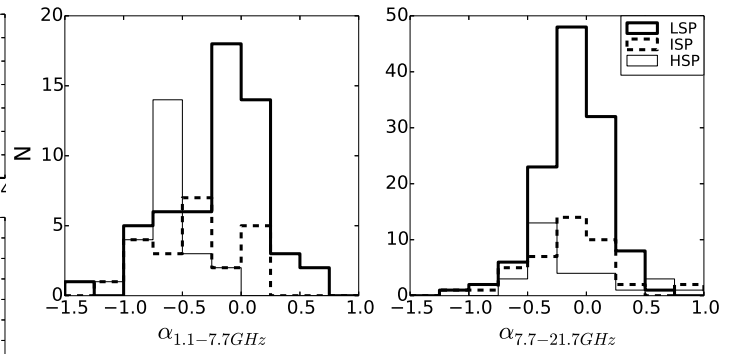


Fig. 3 Distribution of the *average* low and high frequency spectral indices by SED subclass.

nificantly brighter than HSPs and ISPs at all frequencies ($P < 0.001$).

We included the medians of the flux density values at 37 GHz in Table 2. These data come from the brightest sources at this frequency, for example, only for 4 HSP objects and 10 ISP. This can obviously bias the interpretation, so the flux at 37 GHz looks high in general.

4.2 Spectral indices

We calculated spectral indices for the frequency intervals 1.1-7.7 and 7.7-21.7 GHz to investigate the spectral behavior of blazars at low and high frequencies. We used spectral indices measured in the 1.1-7.7 GHz and in 7.7-21.7 GHz frequency intervals as the base range. We also take the indices in the 2.3-7.7 GHz and in 7.7-11.2 GHz range as low and high frequency spectral indices for some sources that did not have measurements in the base range to increase the significance of the statistics. The spectral index α ($S \propto \nu^\alpha$) was calculated by:

$$\alpha = \frac{\log S_2 - \log S_1}{\log \nu_2 - \log \nu_1}, \quad (1)$$

where S_1 is the flux density at the frequency ν_1 , and S_2 the flux density at the frequency ν_2 . Indices were calculated for $S/N > 4$ detections only.

We present results for *average* and *instantaneous* low and high frequency spectral indices.

The *average* spectral indices are listed in Table 3. Fig. 3 shows the distribution of the average spectral index across the sample. We have found that the spectrum of all three types of blazars we considered flattens at the higher frequencies. The spectral indices are closer to zero and have less scatter in 7.7-21.7 GHz and 11.2-37 GHz intervals in comparison to index measured in 1.1-7.7 GHz frequency range. Some care is required in interpreting this result, because of the data at 37 GHz and relatively high variability indices at 21.7 and 37 GHz (see Table 5 in the next subsection).

Now we will describe results on *instantaneous* low and high frequency spectral indices for blazars in our sample.

Table 2 The medians of the flux density values for the SED classes for each frequency, N is the number of sources used to estimate the medians that were calculated for $S/N > 4$ detections only (the brightest source 3C84 was excluded from calculation).

Class	$S_{1.1}$ [Jy]	N	$S_{2.3}$ [Jy]	N	$S_{4.8}$ [Jy]	N	$S_{7.7}$ [Jy]	N	$S_{11.2}$ [Jy]	N	$S_{21.7}$ [Jy]	N	S_{37} [Jy]	N
HSP	0.27	25	0.09	33	0.06	73	0.06	64	0.06	55	0.16	30	0.64	4
ISP	0.53	22	0.42	25	0.35	63	0.31	56	0.30	52	0.38	43	0.63	10
LSP	0.54	56	0.72	61	0.68	153	0.73	146	0.68	141	0.71	121	1.37	43

Table 3 Average and median spectral indices by classes for 1.1-7.7, 7.7-21.7 and 7.7-37 GHz frequency intervals. N - is the number of the *instantaneous* measurements used for calculations.

Class	N	α average	α median
1.1 – 7.7 GHz			
HSP	55	-0.61	-0.55
ISP	65	-0.28	-0.26
LSP	190	-0.05	-0.03
7.7 – 21.7 GHz			
HSP	85	-0.27	-0.30
ISP	154	-0.19	-0.16
LSP	668	-0.12	-0.10
7.7 – 37 GHz			
HSP	25	-0.15	-0.14
ISP	29	0.03	-0.01
LSP	265	0.01	0.02

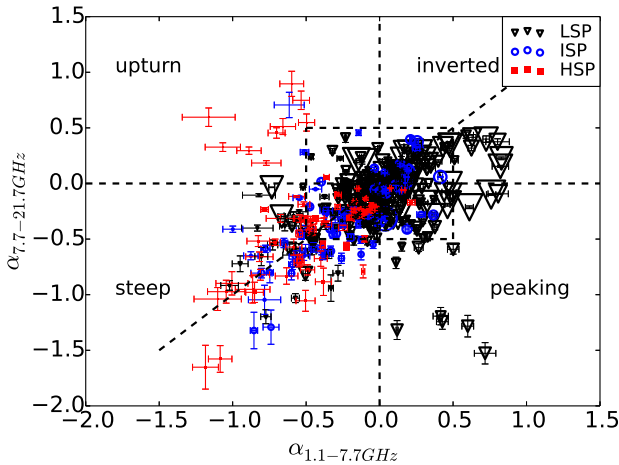


Fig. 4 The “radio colour” plot for *instantaneous* low and high frequency spectral indices. Black reverse triangles denote LSPs, blue circles - ISPs and red squares for HSPs. The size of the marks is related to the flux density at 7.7 GHz.

The *instantaneous* spectral index term refers to a spectral index obtained at one epoch, thus the number of the *instantaneous* spectral indices is equal to the number of epochs of observations for each source. We plotted the *instantaneous* low and high frequency spectral indices in a two-colour diagram (or “radio colour”) in Fig. 4. This kind of representation has been previously used by, e.g., Sadler et al. (2006)

and Tucci et al. (2008). It is a convenient way to describe the shape of the radio spectrum. The dashed lines divide the diagram into four quadrants signifying a steep, upturning, inverted or peaking spectra as marked in the figure. The dashed inclined line is an one-to-one correspondence line, which is an indicator of the spectral behavior. The position of points relative to this line reflects the character of the spectral slope change (steeper or flatter). The box in the center of the plot denotes an area for the flat spectra (with $|\alpha_{radio}| < 0.5$), it is usually referred as the “blazar box”. Most of the spectra corresponding to LSPs (82 %) and ISPs (63 %) are flat, while only 41 % of HSPs have a flat spectrum. For 44 % of HSPs and 34 % of the ISPs the low frequency spectrum is, in fact, steep. Table 4 lists the number of objects in each segment of the plot: inside the blazar box (flat spectrum), and in each quadrant outside the blazar box.

For 35 out of 63 HSPs the spectrum turns flatter at 7.7 GHz, i.e., they are situated above the one-to-one correspondence line in Fig. 4. Nine HSP sources even have a clear upturn. The behaviour of ISPs and LSPs is different: for more than a half of LSPs (183/250) and ISPs (48/70) the spectrum turns steeper at 7.7 GHz. HSPs show more often spectral flattening beyond 7.7 GHz (or even inverted), while the LSP spectra get steeper at that point. LSPs and HSPs clearly occupy different regions of the two-colour plot, with LSPs confined to the right edge and reaching high values of spectral indices ($\alpha_{radio} > -0.5$), while HSPs generally fall into “steep” and “upturn” quadrant.

Kruskal-Wallis pairwise comparisons confirm that the distributions of the distances from the one-to-one line are not significantly different either for HSPs and ISPs or ISPs and LSPs, but instead are significantly different for HSPs and LSPs ($P = 0.05$).

The Pearson product-moment correlation coefficient between the *instantaneous* low and high frequency spectral indices is relatively high and significant only for ISPs ($r = 0.60$). The Spearman rank correlation coefficient values are: 0.28 for HSPs, 0.63 for ISPs and 0.37 for LSPs; and significant (at the 0.05 level) only for ISPs and LSPs. The correlation means that the typical radio spectrum of ISPs and LSPs can be better approximated with a single power-law, while such a model does not describe HSPs spectra accurately.

From both Fig. 3 and Fig. 4 it is clear that the three SED classes have different distributions of the low and high frequency spectral indices, that fact is confirmed by the

Table 4 Blazars distribution in the “radio colour” plot in Fig. 4 by type of the radio spectrum: flat, inverted, peaking, steep or upturn. “Flat” radio spectrum refers to objects inside the blazar box, with $|\alpha_{radio}| < 0.5$. The number of measured *instantaneous* spectral indices for each blazar subclass is presented, the fraction of measurements belonging to the specific spectrum type of is given in brackets.

Spectral shape	Number of indices		
	LSP	ISP	HSP
flat	206 (82%)	44 (63%)	26 (41%)
inverted	7 (3%)	0 (0%)	0 (0%)
peaking	12 (5%)	0 (0%)	0 (0%)
steep	25 (10%)	24 (34%)	28 (44%)
upturn	0 (0%)	2 (3%)	9 (14%)

Kruskall-Wallis test. The difference is also evident in the *average* spectral indices in Table 3.

4.3 Variability

In order to characterize the variability properties of the sources at the various frequencies we have computed the variability and modulation indices. The first one takes into account measurement uncertainties, while the modulation index is less sensitive to outliers. The variability index was calculated as (Aller et al. 1992):

$$V_S = \frac{(S_{max} - \sigma_{S_{max}}) - (S_{min} + \sigma_{S_{min}})}{(S_{max} - \sigma_{S_{max}}) + (S_{min} + \sigma_{S_{min}})} \quad (2)$$

where S_{max} and S_{min} are the maximum and minimum value of the flux density, respectively, at all epochs of observations; $\sigma_{S_{max}}$ and $\sigma_{S_{min}}$ are their errors. This prevents one from overestimating V_S when there are observations with large uncertainties in the dataset. The negative value of V_S corresponds to the case where the flux error is greater than the observed scatter in the data.

The modulation index, defined as the standard deviation of the flux density divided by the mean flux density, was calculated as in Kraus et al. 2003:

$$M = \frac{\sqrt{\frac{1}{N} \sum_{i=1}^N (S_i - \frac{1}{N} \sum_{i=1}^N S_i)^2}}{\frac{1}{N} \sum_{i=1}^N S_i} \quad (3)$$

The medians of the variability and modulation indices for the SED classes by frequency are listed in Table 5. Almost 50 % of HSP objects, 48 % of ISPs, and 56 % of LSPs show variability $M \geq 0.2$. At high frequencies (7.7, 11.2 and 21.7 GHz) only a small number of each type of blazar show variability above 0.7-0.8. The most variable object at all frequencies except 1.1 GHz is AO 0235+164 (27 epochs at high frequencies). It has a bright peaking spectrum at two epochs due to a passing flare in addition to the generally flat spectrum. A large number of observations increases the probability of finding it in active states, such as

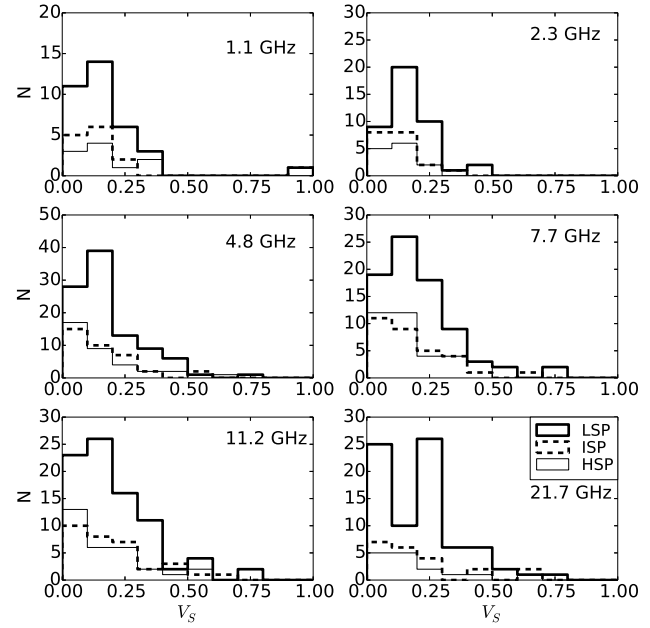


Fig. 5 The variability index distributions at the RATAN frequencies by SED subclass.

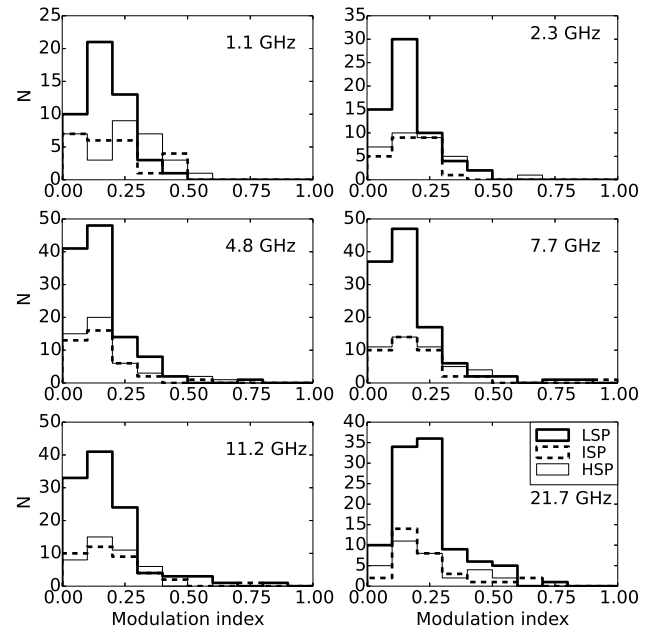


Fig. 6 The modulation index distributions at the RATAN frequencies by SED subclass.

the two peaking spectra contributing to the high variability index. However, at 1.1 GHz the source has little variability. The most variable source at 1.1 GHz is 2E 0323+0214 with $M_{1.1}=0.54$.

The HSPs and ISPs have lower values of the modulation index at six frequencies than LSPs. On the whole, blazars of all three types are less variable at 4.8 GHz, according to the median values of both the modulation and the variability indices. The modulation indices are not drawn from the same

Table 5 The medians of the variability V_S and modulation indices M for three blazar subclasses. N is the number of epochs used to estimate the medians.

Class	1.1 GHz		2.3 GHz		4.8 GHz		7.7 GHz		11.2 GHz		21.7 GHz		37 GHz	
	N	M	N	M	N	M	N	M	N	M	N	M	N	M
HSP	30	0.15	34	0.14	49	0.11	47	0.12	43	0.13	32	0.19	3	0.20
ISP	24	0.16	24	0.14	39	0.11	39	0.12	38	0.12	31	0.18	5	0.27
LSP	48	0.17	61	0.14	114	0.12	113	0.13	110	0.14	101	0.21	30	0.21

Class	1.1 GHz		2.3 GHz		4.8 GHz		7.7 GHz		11.2 GHz		21.7 GHz		37 GHz	
	N	V_S	N	V_S	N	V_S	N	V_S	N	V_S	N	V_S	N	V_S
HSP	30	0.15	34	0.10	49	0.10	47	0.14	43	0.11	32	0.13	3	0.10
ISP	24	0.15	24	0.10	39	0.11	39	0.13	38	0.17	31	0.17	5	0.19
LSP	48	0.17	61	0.17	114	0.14	113	0.17	110	0.17	101	0.20	30	0.29

distribution only at low frequencies (1.1 and 2.3 GHz) for the LSP and HSP classes according to the Kruskal-Wallis test.

5 Discussion

We find interesting differences between the blazar classes in the radio colour plot (Fig. 4). Almost half of HSPs (28 out of 63) in the sample are found to be steep spectrum sources. Only the minority of LSPs and ISPs (25/250 and 24/70, respectively) fall into “steep” quadrant, the most of them have a flat radio spectrum. The latter is not surprising, because a flat radio spectrum was a standard selection criterion of the early radio-selected BL Lac samples. Most of those sources are today classified as LSPs.

The results obtained in this study indicate that the steep and flattening spectra of HSPs is real. One possibility is that there is an extended component in HSP BL Lacs producing optically thin synchrotron radiation, while the flat radio spectrum of LSP BL Lacs can be explained by the compact nuclear core emission. Chhetri et al. (2012) investigated the dependence between the core/extended morphology and radio spectral indices using 20 GHz data from the Australia Telescope Compact Array for the AT20G sample. They conclude that $\alpha = -0.46$ is an effective division point between the compact and extended sources. They also note that a considerable fraction of the extended sources (i.e., $\alpha < -0.46$) show spectral flattening in the higher frequencies. These sources are presumed to be composed of a compact core with an extended component, such as a steep-spectrum quiet jet, lobe or a hot spot. At high radio frequencies this steep spectrum component weakens while the compact, flat spectrum component strengthens, and we observe this as spectral flattening. This situation could happen if the jet is not aligned with the observers line of sight, but the viewing angle is still not very big (close to 30° in case of BL Lacs (Ghisellini et al. (1993); Jackson & Wall (1999)). That explains the flattening of HSPs in our sample.

The largest variability in synchrotron radiation is observed after the peak. Assuming that the flat radio spectrum is a result of superimposed individual synchrotron components, the variability should, on average, increase toward higher frequencies. That is observed in all three types of blazars in our sample at 4.8-21.7 GHz (for LSPs even until

37 GHz) (see Table 5). Secondly, according to our data, both variability and modulation indices for HSPs at all seven frequencies (except the modulation index at 2.3 GHz) are less than for LSPs. That result is also expected, because sources with flat spectrum are more variable than sources with steep spectrum, this result is also in good agreement with Bolton et al. (2006); Sadler et al. (2006); Tucci et al. (2008).

6 Summary

We have presented the results of an observational campaign on BL Lac blazars carried out between 2005 and 2014 with the RATAN-600 radio telescope. The flux densities at frequencies 1.1, 2.3, 4.8, 7.7, 11.2 and 21.7 GHz were measured at several epochs simultaneously. This data set gives us the opportunity to investigate the differences in the radio spectra of all BL Lac types, including the radio-faint HSPs that are rarely targeted by radio studies. We have made two main conclusions:

1. LSP and HSP BL Lac blazars are quite different objects on average. LSPs have higher flux densities (the median of the flux density value is $S_{7.7}=0.73$ Jy), flatter spectra and their variability increases towards higher frequencies. HSPs are very faint in radio domain (the median is $S_{7.7}=0.06$ Jy), tend to have steep low frequency spectra, and they are less variable than LSPs at all frequencies.
2. LSP blazars have flat radio spectra at both low and high frequency ranges that we considered, while the steep low frequency spectra of HSPs (and ISPs) turns flatter above 7.7 GHz. But despite the considerable decrease in the spectral index (“flattening”) at higher frequencies in HSPs, we note that the spectrum of LSPs is still flatter than HSPs.

Acknowledgements. The RATAN-600 observations were carried out with the financial support of the Ministry of Education and Science of the Russian Federation (14.518.11.7054) and Russian Foundation for Basic Research (12-02-31649). The authors (MGM, TVM) acknowledge support through the Russian Government Program of Competitive Growth of Kazan Federal University.

References

- Abdo, A. A., Ackermann, M., Agudo, I., et al. 2010, *ApJ*, 716, 30
- Ackermann, M., Ajello, M., Atwood, W. B., et al. 2015, *ApJ*, 810, 14
- Aller, M. F., Aller, H. D., & Hughes, P. A. 1992, *ApJ*, 399, 16
- Aller, M. F., Aller, H. D., Hughes, P. A., & Latimer, G. E. 1999, *ApJ*, 512, 601
- Antón, S. & Browne, I. W. A. 2005, *MNRAS*, 356, 225
- Baars, J. W. M., Genzel, R., Pauliny-Toth, I. I. K., & Witzel, A. 1977, *A&A*, 61, 99
- Bach, U., Raïteri, C. M., Villata, M., et al. 2007, *A&A*, 464, 175
- Blandford, R. D. & Rees, M. J., eds. 1978, Some comments on radiation mechanisms in Lacertids
- Bolton, R. C., Chandler, C. J., Cotter, G., et al. 2006, *MNRAS*, 370, 1556
- Chhetri, R., Ekers, R. D., Mahony, E. K., et al. 2012, *MNRAS*, 422, 2274
- Ghisellini, G., Padovani, P., Celotti, A., & Maraschi, L. 1993, *ApJ*, 407, 65
- Jackson, C. A. & Wall, J. V. 1999, *MNRAS*, 304, 160
- Kollgaard, R. I. 1994, *Vistas in Astronomy*, 38, 29
- Korolkov, D. V. & Pariiskii, I. N. 1979, *S&T*, 57, 324
- Kraus, A., Krichbaum, T. P., Wegner, R., et al. 2003, *A&A*, 401, 161
- Lister, M. L., Aller, M. F., Aller, H. D., et al. 2013, *AJ*, 146, 120
- Marcha, M. J. M., Browne, I. W. A., Impey, C. D., & Smith, P. S. 1996, *MNRAS*, 281, 425
- Massaro, E., Giommi, P., Leto, C., et al. 2009, *A&A*, 495, 691
- Massaro, E., Maselli, A., Leto, C., et al. 2015, *Ap&SS*, 357, 75
- Mingaliev, M. G., Sotnikova, Y. V., Bursov, N. N., Kardashev, N. S., & Larionov, M. G. 2007, *AZh*, 51, 343
- Mingaliev, M. G., Sotnikova, Y. V., Torniaainen, I., Tornikoski, M., & Udovitskiy, R. Y. 2012, *A&A*, 544, A25
- Mingaliev, M. G., Sotnikova, Y. V., Udovitskiy, R. Y., et al. 2014, *A&A*, 572, A59
- Mücke, A. & Protheroe, R. J. 2001, *Astroparticle Physics*, 15, 121
- Nieppola, E., Tornikoski, M., & Valtaoja, E. 2006, *A&A*, 445, 441
- Ott, M., Witzel, A., Quirrenbach, A., et al. 1994, *A&A*, 284, 331
- Parijskij, Y. N. 1993, *IEEE Antennas and Propagation Magazine*, 35, 7
- Perlman, E. S., Padovani, P., Giommi, P., et al. 1998, *AJ*, 115, 1253
- Petropoulou, M., Dimitrakoudis, S., Padovani, P., Mastichiadis, A., & Resconi, E. 2015, *MNRAS*, 448, 2412
- Richards, J. L., Max-Moerbeck, W., Pavlidou, V., et al. 2011, *ApJS*, 194, 29
- Sadler, E. M., Ricci, R., Ekers, R. D., et al. 2006, *MNRAS*, 371, 898
- Sambruna, R. M., Maraschi, L., & Urry, C. M. 1996, *ApJ*, 463, 444
- Shaw, M. S., Romani, R. W., Cotter, G., et al. 2012, *ApJ*, 748, 49
- Sikora, M., Begelman, M. C., & Rees, M. J. 1994, *ApJ*, 421, 153
- Stickel, M., Padovani, P., Urry, C. M., Fried, J. W., & Kuehr, H. 1991, *ApJ*, 374, 431
- Strittmatter, P. A., Serkowski, K., Carswell, R., et al. 1972, *ApJ*, 175, L7
- Tabara, H. & Inoue, M. 1980, *A&AS*, 39, 379
- Teraesranta, H., Tornikoski, M., Mujunen, A., et al. 1998, *A&AS*, 132, 305
- Teräsanta, H., Achren, J., Hanski, M., et al. 2004, *A&A*, 427, 769
- Tsybulev, P. G. 2011, *Astrophysical Bulletin*, 66, 109
- Tucci, M., Rubiño-Martín, J. A., Rebolo, R., et al. 2008, *MNRAS*, 386, 1729
- Urry, C. M. & Padovani, P. 1995, *PASP*, 107, 803
- Verkhodanov, O. V. 1997, *Astronomical Data Analysis Software and Systems VI*, A.S.P. Conference Series, 125, 46

Table 6 Blazar sample and some parameters.

Source	R.A. (J2000)	Dec (J2000)	N	z	$\log \nu_{peak}^S$	SED class	AGN class
NRAO 5	00:06:13.9	-06:23:35	15	0.347	13.16	LSP*	BL Lac
MS 0011.7+0837	00:14:19.7	+08:54:01	6	0.162	12.44	LSP*	BL.gal.domin
PKS 0017+200	00:19:37.8	+20:21:45	3	0	12.32	LSP	BL Lac
PKS 0019+058	00:22:32.5	+06:08:05	16	0	13.11	LSP	BL Lac
2MASX J00323309-2849200	00:32:33.0	-28:49:20	1	0.324	14.70	ISP	BL Lac
RXS J0325.2+1515	00:35:14.9	+15:15:04	8	1.280	15.10	HSP	BL Lac
1ES 0037+405	00:40:13.7	+40:50:04	1	0	13.16	LSP*	bl.un
RXS J0045.3+2127	00:45:19.2	+21:27:42	1	0	16.00	HSP	BL Lac
PKS 0047+023	00:49:43.3	+02:37:04	11	0	13.63	LSP	BL Lac
PKS 0048-097	00:50:41.2	-09:29:06	14	0.200	14.61	ISP	BL Lac
NPM1G -09.0033	00:56:20.0	-09:36:29	3	0.103	15.55	HSP	BL.gal.domin
RXS J0058.2+1723	00:58:16.7	+17:23:13	2	0	16.28	HSP*	BL Lac
B2 0103+33	01:06:00.2	+34:02:03	1	0.579	13.52	LSP*	bl.un
Q J0109+181	01:09:08.1	+18:16:07	1	0.145	15.02	HSP	BL Lac
NPM1G +41.0022	01:10:04.7	+41:49:50	1	0.096	13.37	LSP*	BL.gal.domin
1FGL J0110.0+6806	01:10:12.8	+68:05:41	1	0.290	14.86	ISP	bl.un
S4 0108+38	01:11:37.3	+39:06:28	12	0.668	12.24	LSP*	bl.un
S2 0109+22	01:12:05.8	+22:44:38	1	0.265	14.33	ISP	BL Lac
PKS 0118-272	01:20:31.6	-27:01:24	3	0.560	14.33	ISP	BL Lac
1ES 0120+340	01:23:08.5	+34:20:47	1	0.272	17.46	HSP	BL Lac
MS 0122.1+0903	01:24:44.5	+09:18:49	3	0.338	13.75	LSP*	BL Lac
PKS 0138-097	01:41:25.8	-09:28:43	13	0.733	13.04	LSP	BL Lac
PKS 0140-059	01:42:38.8	-05:44:01	1	0	13.56	LSP*	BL Lac
1ES 0145+138	01:48:29.7	+14:02:18	8	0.125	14.27	ISP	BL.gal.domin
8C 0149+710	01:53:25.8	+71:15:06	2	0.022	15.69	HSP	BL.gal.domin
87GB 0156.9+1032	01:59:34.4	+10:47:07	6	0.195	16.03	HSP	BL Lac
MS 0158.5+0019	02:01:06.1	+00:34:00	4	0.298	16.82	HSP*	BL Lac
PKS 0202+14	02:04:50.4	+15:14:11	4	0.833	12.71	LSP	bl.un
S5 0205+72	02:09:51.7	+72:29:26	1	0.895	12.71	LSP*	bl.un
Z 0214+083	02:17:17.0	+08:37:03	7	1.400	13.79	LSP	BL Lac
OD 330	02:21:05.5	+35:56:13	2	0.944	13.16	LSP	bl.un
PKS 0219-164	02:22:00.7	-16:15:16	1	0.698	14.58	ISP	FSRQ
3C 66A	02:22:39.6	+43:02:07	5	0.444	15.09	HSP	BL Lac
1ES 0229+200	02:32:48.6	+20:17:17	5	0.140	15.48	HSP	BL.gal.domin
AO 0235+164	02:38:38.8	+16:36:59	28	0.940	13.31	LSP	BL Lac
PKS 0245-167	02:48:07.7	-16:31:46	3	0	12.84	LSP*	BL Lac
RXS J0250.6+1712	02:50:38.0	+17:12:08	7	1.100	16.41	HSP	bl.un
PKS 0301-243	03:03:26.5	-24:07:13	5	0.260	15.43	HSP	BL Lac
4C 47.08	03:03:35.2	+47:16:16	5	0.475	14.00	ISP	BL Lac
PKS 0306+102	03:09:03.6	+10:29:16	15	0.863	13.14	LSP	FSRQ
RXS J0314.3+0620	03:14:23.9	+06:19:57	5	0	15.92	HSP*	BL Lac
RXS J0316.1+0904	03:16:12.9	+09:04:43	6	0	15.77	ISP	BL Lac
3C 84	03:19:48.1	+41:30:42	6	0.018	13.57	LSP	bl.un
MS 0317.0+1834	03:19:51.8	+18:45:35	6	0.190	16.99	HSP	BL.gal.domin
2E 0323+0214	03:26:13.9	+02:25:14	7	0.147	15.93	HSP	BL Lac
PKS 0338-214	03:40:35.6	-21:19:31	5	0.223	13.49	LSP	BL Lac
PKS 0346-163	03:48:39.2	-16:10:17	8	0	13.45	LSP	BL Lac
S5 0346+800	03:54:46.1	+80:09:28	1	0	12.60	LSP	cand.
PKS 0357-264	03:59:33.6	-26:15:31	3	1.470	13.16	LSP	BL Lac
PKS 0406+121	04:09:22.1	+12:17:39	19	1.020	13.16	LSP*	BL Lac
2E 0414+0057	04:16:52.4	+01:05:24	6	0.287	16.64	HSP	BL Lac
MS 0419.3+1943	04:22:18.5	+19:50:53	2	0.512	12.62	LSP*	BL Lac
PKS 0420+022	04:22:52.2	+02:19:27	9	2.277	12.35	LSP*	FSRQ
PKS 0422+004	04:24:46.8	+00:36:07	14	0.310	14.10	ISP	BL Lac
MCG -01.12.005	04:25:51.3	-08:33:39	4	0.039	12.80	LSP*	BL.gal.domin
3C 120	04:33:11.0	+05:21:15	5	0.033	14.30	ISP*	bl.un
2EG J0432+2910	04:33:37.8	+29:05:55	2	0.970	13.40	LSP	BL Lac
PKS 0439-299	04:41:19.5	-29:52:35	2	0	13.91	LSP*	cand.
PKS 0446+11	04:49:07.6	+11:21:28	20	1.207	12.76	LSP	FSRQ

Table 6 Blazar sample and some parameters. Continued.

Source	R.A. (J2000)	Dec (J2000)	N	z	$\log \nu_{peak}^S$	SED class	AGN class
PKS 0459+135	05:02:33.2	+13:38:11	8	0	13.18	LSP*	BL Lac
Q 0458+6530	05:03:05.8	+65:34:01	1	0	16.45	HSP*	cand.
RXS J0505.5+0416	05:05:34.7	+04:15:54	6	0.027	15.96	HSP	BL Lac
1ES 0502+675	05:07:56.1	+67:37:24	6	0.416	18.20	HSP*	BL Lac
S5 0454+84	05:08:42.3	+84:32:04	3	1.340	13.28	LSP*	BL Lac
MG 0509+0541	05:09:25.9	+05:41:35	3	0	14.22	ISP	BL Lac
4U 0506-03	05:09:39.0	-04:00:36	14	0.304	17.13	HSP*	cand.
1FGL J0515.2+7355	05:16:31.2	+73:51:08	1	0.249	16.02	HSP	BL Lac
PKS 0524+034	05:27:32.7	+03:31:31	7	0	12.94	LSP*	BL Lac
1WGA J0536.4-3342	05:36:29.1	-33:43:02	1	0	16.05	HSP*	BL Lac
HB89 0548-322	05:50:40.6	-32:16:17	1	0.069	17.23	HSP*	BL.gal.domin
B3 0609+413	06:12:51.1	+41:22:37	2	0	14.49	ISP	BL Lac
MS 0607.9+7108	06:13:43.3	+71:07:26	1	0.267	15.00	ISP*	BL Lac
J0617+5701	06:17:16.9	+57:01:16	2	0	13.45	LSP	BL Lac
87GB 06216+4441	06:25:18.2	+44:40:01	7	0	14.55	ISP	BL Lac
PKS 0627-199	06:29:23.7	-19:59:19	1	0	13.23	LSP	BL Lac
1ES 0647+250	06:50:46.5	+25:03:00	2	0.203	16.42	HSP	BL Lac
B3 0651+428	06:54:43.5	+42:47:58	1	0.126	13.01	LSP*	BL.gal.domin
4C +42.22	06:56:10.6	+42:37:02	5	0.059	15.39	HSP	BL.gal.domin
2MASS J06562263-2403194	06:56:22.6	-24:03:19	1	0.371	15.30	HSP*	BL Lac
J0707+6110	07:07:00.6	+61:10:11	3	0	13.48	LSP*	BL Lac
EXO 0706.1+5913	07:10:30.1	+59:08:21	6	0.125	16.99	HSP	BL Lac
B3 0707+476	07:10:46.1	+47:32:11	2	1.292	13.24	ISP	BL Lac
GB2 0716+332	07:19:19.4	+33:07:09	1	0.779	14.08	ISP	FSRQ
S5 0716+714	07:21:53.4	+71:20:36	6	0.300	13.99	LSP	BL Lac
PKS 0723-008	07:25:50.6	-00:54:56	4	0.128	13.41	LSP	bl.un
PKS 0735+17	07:38:07.4	+17:42:19	15	0.424	13.98	LSP	BL Lac
4C +54.15	07:53:01.3	+53:52:59	3	0.200	13.28	LSP	BL Lac
GB 0751+485	07:54:45.6	+48:23:50	1	0.377	13.84	LSP	BL Lac
PKS 0754+100	07:57:06.7	+09:56:35	24	0.266	13.49	LSP	BL Lac
PKS 0808+019	08:11:26.6	+01:46:52	16	0.930	13.23	LSP	BL Lac
1WGA J0816.0-0736	08:16:04.3	-07:35:59	4	0.040	14.76	ISP	BL.gal.domin
J0817-0933	08:17:49.7	-09:33:30	2	0	14.05	ISP	BL Lac
OJ 425	08:18:16.0	+42:22:45	5	0.530	12.99	LSP	BL Lac
PKS 0818-128	08:20:57.4	-12:58:59	6	0.074	14.72	ISP	BL Lac
4C 22.21	08:23:24.7	+22:23:03	4	0.951	13.27	LSP*	BL Lac
PKS 0823+033	08:25:50.3	+03:09:24	22	0.506	13.18	LSP	BL Lac
PKS 0823-223	08:26:01.5	-22:30:27	3	0.910	14.44	ISP	BL Lac
PKS 0829+046	08:31:48.9	+04:29:39	7	0.174	13.71	LSP	BL Lac
1H 0827+089	08:31:55.1	+08:47:43	5	0.941	13.15	LSP*	FSRQ
OJ 448	08:32:23.2	+49:13:20	2	0.548	12.90	LSP	BL Lac
TEX 0836+182	08:39:30.7	+18:02:47	14	0.280	14.22	ISP	BL Lac
PKS 0837+035	08:39:49.2	+03:19:53	5	1.570	12.79	LSP	BL Lac
RXS J0847.2+1133	08:47:12.9	+11:33:52	4	0.198	15.95	HSP	BL Lac
2MASS J08475674-0703169	08:47:56.7	-07:03:17	1	0	13.53	LSP	BL Lac
US1889	08:54:09.8	+44:08:30	3	0.382	14.16	ISP	BL Lac
OJ 287	08:54:48.8	+20:06:30	11	0.306	13.73	LSP	BL Lac
NPM1G -09.0307	09:08:02.2	-09:59:37	7	0.054	12.91	LSP*	bl.un
3C 216.0	09:09:33.4	+42:53:46	7	0.670	13.31	LSP*	bl.un
RXS J09130-2103	09:13:00.1	-21:03:20	1	0.198	16.50	HSP	BL Lac
B2 0912+29	09:15:52.3	+29:33:24	3	0.101	15.59	HSP	BL Lac
B2 0922+31B	09:25:43.6	+31:27:10	1	0.260	13.27	LSP	BL Lac
J09291544+5013360	09:29:15.4	+50:13:35	4	0.370	14.14	ISP	BL Lac
1ES 0927+500	09:30:37.5	+49:50:25	5	0.188	15.29	HSP	BL Lac
B2 0927+35	09:30:55.2	+35:03:37	10	0	12.67	LSP*	BL Lac
B2 0937+26	09:40:14.7	+26:03:29	5	0.498	13.33	LSP*	BL Lac
RXS J09449-1347	09:44:59.2	-13:47:51	1	0	14.24	ISP*	cand.
2FGL J0945.9+5751	09:45:42.2	+57:57:47	1	0.229	14.73	ISP	BL Lac
RXS J09530-0840	09:53:02.6	-08:40:18	1	0	15.29	HSP	BL Lac
S4 0954+65	09:58:47.2	+65:33:54	6	0.367	13.49	LSP	BL Lac

Table 6 Blazar sample and some parameters. Continued.

Source	R.A. (J2000)	Dec (J2000)	N	z	$\log v_{peak}^s$	SED class	AGN class
4C22.25	10:00:21.9	+22:33:18	7	0.419	14.39	ISP*	bl.un
J1008+0621	10:08:00.8	+06:21:21	2	0.650	14.21	ISP*	BL Lac
RXS J1008.1+4705	10:08:11.3	+47:05:20	3	0.343	14.49	ISP	BL Lac
PKS 1008+013	10:11:15.6	+01:06:42	1	1.275	13.01	LSP*	BL Lac
NRAO 350	10:12:13.3	+06:30:57	11	0.727	14.98	ISP	BL Lac
RXS J1012.7+4229	10:12:44.3	+42:29:57	8	0.364	16.81	HSP	BL Lac
2FGL J1019.8+6322	10:19:50.8	+63:20:01	1	2.025	13.24	LSP	BL Lac
RXS J1022.7-0112	10:22:43.9	-01:13:02	6	0	16.64	HSP	BL Lac
SDSS J10326+6623	10:32:39.0	+66:23:23	1	2.212	14.08	ISP	BL Lac
J1036+1233	10:36:40.3	+12:33:38	1	0	14.35	ISP*	BL Lac
TEX 1040+244	10:43:09.0	+24:08:35	15	0.560	12.77	LSP	FSRQ
S5 1044+719	10:48:27.6	+71:43:35	2	1.150	13.19	LSP	bl.un
GB6 J1054+2210	10:54:30.6	+22:10:54	1	1.539	14.60	ISP	BL Lac
RX J10578-2753	10:57:50.7	-27:54:11	1	0.092	15.64	HSP	BL Lac
B3 1055+433	10:58:02.9	+43:04:41	1	2.204	12.68	LSP*	BL Lac
4C 01.28	10:58:29.6	+01:33:58	8	0.890	13.18	LSP	bl.un
MRK 421	11:04:27.2	+38:12:32	13	0.031	17.07	HSP	BL Lac
RXS J1110.6+7133	11:10:37.5	+71:33:56	1	0	15.55	HSP	BL Lac
FIRST J1117.6+2548	11:17:40.4	+25:48:46	1	0.360	15.60	HSP	BL Lac
EXO 1118	11:20:48.0	+42:12:12	1	0.124	17.18	HSP	BL Lac
CGRaBS J1121-0711	11:21:42.1	-07:11:06	1	0	12.44	LSP*	BL Lac
J112402.70+23	11:24:02.7	+23:36:45	5	1.549	13.12	LSP	FSRQ
J1132+0034	11:32:45.6	+00:34:27	4	1.223	14.07	ISP	BL Lac
MS 1133.7+1618	11:36:17.6	+16:01:53	3	0.574	12.16	LSP*	BL Lac
MRK 180	11:36:26.4	+70:09:27	1	0.045	15.77	HSP	BL Lac
A1137+1544	11:40:23.4	+15:28:09	1	0.244	15.99	HSP	BL Lac
GB6 B1144+3517	11:47:22.1	+35:01:07	2	0.063	14.60	ISP*	BL.gal.domin
J1148+1840	11:48:37.7	+18:40:09	5	0.405	13.10	LSP*	BL Lac
EXO 1149.9+2455	11:49:30.3	+24:39:27	3	0.402	14.61	ISP*	BL Lac
B2 1147+24	11:50:19.2	+24:17:54	15	0.200	14.02	ISP	BL Lac
RXS J1151.4+5859	11:51:24.6	+58:59:17	1	0.118	14.72	ISP	BL Lac
SBS 1200+608	12:03:03.5	+60:31:19	1	0.065	14.93	ISP	BL Lac
J1206+0529	12:06:58.0	+05:29:52	4	0.791	13.85	LSP*	BL Lac
CGRaBS J1209-2032	12:09:14.6	-20:32:39	1	0.404	12.20	LSP*	BL Lac
B3 1206+416	12:09:22.7	+41:19:41	1	0.377	13.85	LSP	BL Lac
IES 1212+078	12:15:10.9	+07:32:04	5	0.136	13.27	LSP*	BL.gal.domin
GB6 B1215+3023	12:17:52.0	+30:07:00	3	0.130	15.26	HSP	BL Lac
PKS 1215-002	12:17:58.7	-00:29:46	1	0.419	13.51	LSP	BL Lac
GB2 1217+348	12:20:08.2	+34:31:21	1	0.643	13.95	LSP	BL Lac
PG 1218+304	12:21:21.9	+30:10:37	5	0.182	16.66	HSP	BL Lac
1WGA J1221.5+2813	12:21:31.6	+28:13:58	6	0.102	14.44	ISP	BL Lac
S5 1221+80	12:23:40.4	+80:40:04	5	0	13.22	LSP	BL Lac
RXS J12302+2517	12:30:14.0	+25:18:06	6	0.135	14.91	ISP	BL Lac
2E 1258+1437	12:31:23.9	+14:21:25	2	0.260	15.03	HSP	BL Lac
BZB J1235+1700	12:35:28.8	+17:00:36	1	0.381	14.01	ISP*	BL.gal.domin
FIRST J1236.3+3900	12:36:23.0	+39:00:01	1	0.390	14.78	ISP	BL Lac
RX J12370+3020	12:37:05.5	+30:20:05	1	0.700	12.20	LSP*	BL Lac
RXS J12416+3440	12:41:41.4	+34:40:31	7	0	12.27	LSP*	BL Lac
IES 1239+069	12:41:48.3	+06:36:01	3	0.150	15.06	HSP	BL Lac
RX J12418-1455	12:41:49.3	-14:55:58	1	0	15.88	HSP	BL Lac
Ton 116	12:43:12.7	+36:27:43	3	1.065	16.15	HSP	BL Lac
S5 1250+53	12:53:11.9	+53:01:11	5	1.084	13.94	LSP	BL Lac
PKS 1256-229	12:59:08.4	-23:10:38	1	0.481	13.62	LSP	bl.un

Table 6 Blazar sample and some parameters. Continued.

Source	R.A. (J2000)	Dec (J2000)	N	z	$\log \nu_{peak}^S$	SED class	AGN class
FIRST J1301.7+4056	13:01:45.6	+40:56:24	1	0.649	13.04	LSP*	BL Lac
GB6 B1300+5804	13:02:52.4	+57:48:37	2	1.088	12.28	LSP	bl.un
RXS J1302.9+5056	13:02:55.5	+50:56:17	1	0.688	12.42	LSP*	BL Lac
MC2 1307+12	13:09:33.9	+11:54:24	14	0.318	13.32	LSP	BL Lac
OP 313	13:10:28.6	+32:20:43	10	0.997	13.30	LSP	bl.un
PKS 1309-216	13:12:31.5	-21:56:24	1	1.491	15.46	HSP	BL Lac
RXS J1319.5+1405	13:19:31.7	+14:05:34	5	0.572	15.49	HSP	BL Lac
J132247.40+3216	13:22:47.3	+32:16:08	5	0	15.13	HSP*	BL Lac
RXS J1326.2+1230	13:26:17.6	+12:29:58	5	0.204	12.33	LSP*	BL.gal.domin
J132952.86+3154	13:29:52.8	+31:54:11	1	0	12.44	LSP*	cand.
SDSS J13338+5057	13:33:53.7	+50:57:36	1	1.362	14.32	ISP	bl.un
MS1332.6-2935	13:35:29.7	-29:50:39	1	0.513	14.86	ISP	BL Lac
RXS J1341.0+3959	13:41:05.0	+39:59:45	6	0.172	14.63	ISP	BL.gal.domin
J134916-141316	13:49:16.0	-14:13:17	1	0.253	13.20	LSP*	BL Lac
PKS1350+148	13:53:22.8	+14:35:39	2	0.807	13.57	LSP	BL Lac
RXS J1353.4+5601	13:53:28.0	+56:00:56	2	0.404	12.18	LSP*	BL Lac
MC 1400+162	14:02:44.5	+15:59:57	12	0.244	14.44	ISP*	BL Lac
MS 1402.3+0416	14:04:51.0	+04:02:02	5	0.344	15.83	HSP	BL Lac
MS 1407.9+5954	14:09:23.4	+59:39:40	1	0.496	15.04	HSP*	BL Lac
PKS 1407+022	14:10:04.6	+02:03:06	10	0	13.24	LSP*	BL Lac
RXS J1410.5+6100	14:10:31.7	+61:00:10	5	0.384	14.93	ISP*	BL Lac
PKS 1413+135	14:15:58.8	+13:20:24	11	0.247	12.96	LSP	bl.un
2E 1415+2557	14:17:56.6	+25:43:25	2	0.237	15.45	HSP	BL Lac
OQ 530	14:19:46.6	+54:23:14	4	0.153	13.98	LSP	BL Lac
SDSS J14202+0614	14:20:13.6	+06:14:28	1	0.625	13.49	LSP*	BL Lac
PKS 1424+240	14:27:00.5	+23:48:00	11	0.160	15.34	HSP	BL Lac
RXS J1436.9+5639	14:36:57.7	+56:39:24	1	0.150	16.88	HSP	BL Lac
PKS 1437-153	14:39:56.8	-15:31:50	7	0.636	13.46	LSP	BL Lac
1ES 1440+122	14:42:48.3	+12:00:40	6	0.162	16.35	HSP	BL Lac
RXS J14495+2746	14:49:32.6	+27:46:21	1	0.227	12.40	LSP*	BL.gal.domin
B2 1451+26	14:53:53.5	+26:48:33	3	0	13.12	LSP*	bl.un
RXS J1456.0+5048	14:56:03.7	+50:48:25	5	0.480	12.52	LSP*	BL Lac
RXS J1458.4+4832	14:58:27.0	+48:32:46	2	0.541	15.44	HSP*	BL Lac
B3 1456+375	14:58:44.8	+37:20:22	8	0.333	13.31	LSP	BL Lac
TXS 1459+480	15:00:48.6	+47:51:15	1	1.059	13.15	LSP	FSRQ
PKS 1514+197	15:16:56.8	+19:32:12	19	0.650	12.97	LSP	BL Lac
PKS 1514-24	15:17:41.8	-24:22:19	4	0.048	14.19	ISP	BL Lac
PKS 1519-273	15:22:37.6	-27:30:10	5	1.294	12.79	LSP	BL Lac
1ES 1533+535	15:35:00.8	+53:20:37	5	0.890	16.99	HSP	BL Lac
MS 1534.2+0148	15:36:46.8	+01:37:59	5	0.311	14.64	ISP*	BL Lac
4C 14.60	15:40:49.4	+14:47:45	20	0.605	13.53	LSP	BL Lac
RXS J1542.9+6129	15:42:56.9	+61:29:55	2	0.117	14.64	ISP	BL Lac
RXS J1544.3+0458	15:44:18.7	+04:58:22	6	0.326	12.80	LSP*	BL.gal.domin
PG 1553+11	15:55:43.1	+11:11:24	10	0.326	14.12	ISP	BL Lac
MYC 1557+566	15:58:48.2	+56:25:14	1	0.300	14.21	ISP	BL Lac
CGRaBS J1603+1105	16:03:41.9	+11:05:48	7	0.143	13.46	LSP	BL Lac
PKS 1604+159	16:07:06.4	+15:51:34	10	0.357	13.36	LSP	BL Lac
RXS J1610.0+6710	16:10:04.1	+67:10:26	1	0.067	16.20	HSP*	BL Lac
SDSS J16183+3632	16:18:23.5	+36:32:01	3	0.730	13.43	LSP*	BL Lac
NGC 6251	16:32:31.9	+82:32:16	3	0.025	13.73	LSP	bl.un
CGRaBS J1642-0621	16:42:02.1	-06:21:23	4	1.514	13.23	LSP	BL Lac
1FGL J1647.4+4948	16:47:34.9	+49:50:00	1	0.047	13.70	LSP	bl.un
PKS 1648+015	16:51:03.6	+01:29:23	4	0.400	12.88	LSP*	BL Lac
MRK 501	16:53:52.2	+39:45:36	12	0.033	16.12	HSP	BL Lac
SDSS J16581+6150	16:58:08.3	+61:50:02	1	0.374	14.62	ISP	BL Lac

Table 6 Blazar sample and some parameters. Continued.

Source	R.A. (J2000)	Dec (J2000)	N	z	$\log \nu_{peak}^S$	SED class	AGN class
PKS 1707-038	17:10:17.2	-03:55:50	9	1.920	12.78	LSP*	FSRQ
PGC 59947	17:15:22.9	+57:24:40	1	0.027	-	-	BL.gal.domin
TEX 1714-336	17:17:36.0	-33:42:08	3	0	13.08	LSP*	cand.
PKS 1717+177	17:19:13.1	+17:45:06	11	0.137	13.33	LSP*	BL Lac
H 1722+119	17:25:04.4	+11:52:16	6	0.018	16.01	HSP	BL Lac
BZB J1733+4519	17:33:28.8	+45:19:50	1	0.317	-	-	BL.gal.domin
OT 465	17:39:57.1	+47:37:58	1	0.950	13.19	LSP	BL Lac
NPM1G +19.0510	17:43:57.9	+19:35:09	7	0.083	15.76	HSP	BL.gal.domin
J1745-0753	17:45:27.1	-07:53:03	7	0	13.36	LSP	BL Lac
B2 1743+39C	17:45:37.6	+39:51:31	3	0.267	15.15	HSP	BL.gal.domin
S4 1749+70	17:48:32.8	+70:05:50	3	0.770	13.78	LSP	BL Lac
PKS 1749+096	17:51:32.7	+09:39:01	17	0.322	12.41	LSP	BL Lac
RXS J1756.2+5522	17:56:15.9	+55:22:18	5	0.407	16.46	HSP	BL Lac
S5 1803+78	18:00:45.6	+78:28:04	5	0.680	13.55	LSP	BL Lac
3C 371	18:06:50.6	+69:49:28	3	0.046	14.69	ISP	BL Lac
4C 56.27	18:24:07.0	+56:51:01	3	0.664	13.19	LSP	BL Lac
3C 380.0	18:29:31.7	+48:44:46	3	0.695	13.27	LSP	bl.un
1H 1914-194	19:17:44.8	-19:21:30	1	0.137	15.41	HSP	BL Lac
S4 1926+61	19:27:30.4	+61:17:31	1	0	13.36	LSP	BL Lac
S5 2007+77	20:05:30.9	+77:52:43	6	0.342	13.53	LSP	BL Lac
4C +72.28	20:09:52.3	+72:29:19	2	0	12.90	LSP	BL Lac
PKS 2012-017	20:15:15.1	-01:37:33	6	0.520	14.43	ISP	BL Lac
S5 2023+76	20:22:35.5	+76:11:26	5	0.594	14.11	ISP	BL Lac
PKS 2029+121	20:31:54.9	+12:19:41	2	1.215	12.95	LSP	bl.un
PKS 2032+107	20:35:22.3	+10:56:06	6	0.601	14.03	ISP	FSRQ
IES 2037+521	20:39:23.5	+52:19:49	1	0.053	16.47	HSP	cand.
PKS 2047+039	20:50:06.2	+04:07:49	12	0	13.08	LSP	BL Lac
S5 2051+74	20:51:33.7	+74:41:40	1	0	12.76	LSP*	cand.
GB6 J2116+3339	21:16:14.5	+33:39:20	1	0.350	15.33	HSP	BL Lac
PKS 2131-021	21:34:10.2	-01:53:17	14	0.557	13.19	LSP	BL Lac
MS 2143.4+0704	21:45:52.3	+07:19:27	5	0.237	14.58	ISP	BL Lac
PKS 2149+17	21:52:24.8	+17:34:37	15	0.871	13.38	LSP	BL Lac
PKS 2155-304	21:58:52.0	-30:13:32	3	0.116	15.97	HSP	BL Lac
BL LAC	22:02:43.2	+42:16:40	19	0.069	13.39	LSP	BL Lac
B2 2214+24B	22:17:00.8	+24:21:46	5	0.505	13.37	LSP	BL Lac
J221944+212056	22:19:44.1	+21:20:53	2	0.200	13.88	LSP*	BL Lac
PKS 2221-116	22:24:07.9	-11:26:21	2	0.115	13.41	LSP	BL Lac
PKS 2223-114	22:25:43.7	-11:13:41	5	0.997	13.04	LSP*	BL Lac
3C 446	22:25:45.1	-04:56:34	14	1.404	13.32	LSP	FSRQ
FIRST J22279+0037	22:27:58.1	+00:37:05	1	0	14.41	ISP	BL Lac
RXS J2233.0+1335	22:33:01.1	+13:36:02	5	0.214	14.67	ISP*	BL Lac
PKS 2233-173	22:36:09.5	-17:06:21	1	0.647	13.57	LSP	BL Lac
PKS 2233-148	22:36:34.0	-14:33:22	2	0.325	13.08	LSP	BL Lac
B3 2238+410	22:41:07.2	+41:20:11	1	0.726	13.32	LSP	BL Lac
PKS 2240-260	22:43:26.4	-25:44:30	3	0.774	13.22	LSP	BL Lac
RGB J2243+203	22:43:54.7	+20:21:03	1	0	15.58	HSP	BL Lac
B3 2247+381	22:50:05.7	+38:24:37	1	0.119	15.93	HSP*	BL Lac
PKS 2251+006	22:54:04.4	+00:54:20	2	0	12.92	LSP*	BL Lac
PKS 2254+074	22:57:17.3	+07:43:12	7	0.190	13.76	LSP*	BL Lac

Table 6 Blazar sample and some parameters. Continued.

Source	R.A. (J2000)	Dec (J2000)	N	z	$\log \nu_{peak}^s$	SED class	AGN class
RXS J2304.6+3705	23:04:36.6	+37:05:08	7	0	15.88	HSP	BL Lac
PGC 1465934	23:13:57.3	+14:44:23	1	0.163	15.42	HSP	BL.gal.domin
Q J2319+161	23:19:43.4	+16:11:50	2	0	12.63	LSP*	BL Lac
GB6 J2325+3957	23:25:17.8	+39:57:37	1	0	13.71	LSP	BL Lac
IES 2326+174	23:29:03.3	+17:43:30	5	0.213	15.62	HSP*	BL Lac
Q J2338+212	23:38:56.4	+21:24:41	5	0.291	14.83	ISP	cand.
MS 2336.5+0517	23:39:07.0	+05:34:36	2	0.740	15.95	HSP*	BL Lac
B2 2337+26	23:40:29.0	+26:41:56	6	0.372	12.42	LSP*	cand.
1FGL J2341.6+8015	23:40:53.7	+80:15:13	1	0.274	15.64	HSP	BL Lac
MS 2342.7-1531	23:45:22.3	-15:15:06	1	0	16.18	HSP*	FSRQ
MS J23492105+0534	23:49:21.0	+05:34:40	4	0.419	13.58	LSP*	FSRQ
MS 2347.4+1924	23:50:01.7	+19:41:52	4	0.515	13.37	LSP*	bl.un
RXS J2350.3-059	23:50:18.0	-05:59:27	1	0.515	13.89	LSP*	cand.
PKS 2354-02	23:57:25.1	-01:52:15	7	0.812	13.38	LSP	BL Lac

Col. 1 – source name, Col. 2–3 – R.A. and Dec (J2000.0), Col. 4 – number of observing epochs at RATAN, Col. 5 – redshift z (BZCAT or Simbad),

Col. 6 – logarithm of the synchrotron peak frequency ν_{peak}^s in Hz, Col. 7 – SED class from BZCAT or Nieppola et al. (2006), we noted "*" blazars, for which

Col. 8 – AGN class from BZCAT